(Received 5 September 2025, Accepted 21 October 2026, Scheduled 5 April 2026)

High Q-Factor Permittivity Sensor with Dual-Band and Independent Performance for Solid Material Characterization

Leni D. Asrar[1,2], Zahriladha Zakaria[1,*], Syah Alam[3], Iwan Setyadi[4], and Maizatul A. Meor Said[1]

[1] Center for Telecommunication Research and Innovation (CeTRI)
Fakulti Teknologi dan Kejuruteraan Elektronik dan Komputer (FTKEK)
Universiti Teknikal Malaysia Melaka (UTeM), Malaysia
[2] Faculty of Industrial Technology, Institut Teknologi Budi Utomo, Indonesia
[3] Department of Electrical Engineering, Universitas Trisakti, Indonesia
[4] Advanced Materials Research Center-National Research and Innovation Agency (BRIN), Indonesia

ABSTRACT: This study proposes a two-port dual-band microwave sensor designed for the independent and simultaneous detection of solid material characteristics. The sensor consists of a pair of non-identical rectangle-shaped resonators arranged symmetrically, with two distinct sensing areas connected by a power divider and a microstrip feed line with an impedance of 50 Ohms. It operates at resonant frequencies of $f_{r1} = 2.16$ GHz and $f_{r2} = 4.03$ GHz, utilizing a Rogers 5880 substrate with $\varepsilon_r = 2.2$, $\tan\delta = 0.0009$, and a thickness of 0.79 mm. The tested materials include RO5880, RO4350, and FR4, with dimensions of 16 mm $\times$ 5 mm on the first resonator and 5 mm $\times$ 5 mm on the second resonator. The rectangular resonators successfully detect and measure the dielectric properties of solid materials while maintaining independent operation, ensuring that MUT loading does not interfere with each resonator. The measurement results indicate that f_{r1} and f_{r2} achieve average accuracies of 90.51% and 95.16%, respectively, for a permittivity range of 1–4.4, while the average normalized sensitivities are 2.42% and 1.36%. In addition, the Q-factors of resonators are 308 and 537, respectively. The proposed microwave sensor offers a promising solution for accurately detecting different characteristics of solid materials independently and simultaneously, with potential applications in the food industry, material quality control, and biomedical fields.

1. INTRODUCTION

Determining the permittivity characteristics of materials is essential in microwave engineering and plays a pivotal role in numerous applications. Accurate measurement of the dielectric constant, or relative permittivity, is particularly critical in fields such as the food industry, agriculture, medicine, healthcare, and the military and defense sectors [1–3]. In general, the permittivity of the material under test (MUT) can be measured and analyzed using a microwave sensor, including those designed for liquid characterization [4–7], solid materials [8–13], and temperature-dependent measurements [14]. The characteristics and permittivity of a material can be determined using various microwave sensor methods, such as planar resonators [15] and waveguides [16, 17]. Planar resonators offer advantages such as compact design, low production costs, and easy fabrication [5, 6, 18].

To enhance the accuracy and sensitivity of planar resonators, several studies have proposed high-sensitivity microwave sensors for characterizing solid and liquid materials. They include complementary split-ring resonators (CSRRs) [19–23], square split-ring resonators (SSRRs) [24], split-ring resonators (SRRs) [25], interdigital capacitors (IDCs) [26], substrate integrated waveguides (SIWs) [16, 27], interdigital complementary split-ring resonator sensors (ICSRRs) [28], complementary symmetric S-shaped resonators (CSSSRs) [29], complementary symmetric split-ring resonators (CSSRRs) [30], and multiple complementary split-ring resonators (MCSRRs) [31]. Other approaches, such as interdigital structures (IDS) [7], have also been explored. However, previous sensor designs primarily rely on single sensing, making them unsuitable for simultaneous material characterization.

Currently, multi-resonator (dual-band) sensors are being developed to detect multiple materials simultaneously. In previous research, the permittivity of two separate liquid samples at different frequencies was successfully measured simultaneously using an SRR-based microwave sensor [32]. Nevertheless, the sensor is not independent, as placing a sample on the slots of either split-ring resonator (SRR) alters both resonant frequencies. Ref. [33] successfully enhanced sensitivity, achieving frequency shifts of 66 MHz and 116 MHz at resonance frequencies of 1.71 GHz (3G) and 2.35 GHz (4G). Nevertheless, measurements can only be conducted simultaneously on identical materials. Meanwhile, a Hexagonal Split Ring Resonator (HSRR) proposed in [34] demonstrated an exceptionally high normalized sensitivity of 4.646% and an average sensitivity of 246.48 MHz/ε_r. To achieve differential sensing, one of the resonating elements is designated as the reference, while the other serves as the material sensing unit. Furthermore, the dual-band sensor presented in [35] offers an innovative planar cavity design with IDC-SRRs for differential sensing, achieving high sensitivity and distinct frequency splitting. Despite this, the resonance mechanisms are mutually dependent,

* Corresponding author: Zahriladha Zakaria (zahriladha@utem.edu.my).

which constrains the true independence of dual-band operation. In [36], a dual-band microwave sensor is based on an SRR combined with a pair of L-shaped structures. The maximum and average normalized sensitivity (NS) values are 0.073% and 0.06%, respectively. However, the proposed sensor is only for detecting the permittivity of liquids and displacement of solids. Another study proposed a dual-band planar microwave sensor system to independently measure the complex dielectric constant of solid materials with resonant frequency configurations at 3 GHz and 3.92 GHz. However, this system simultaneously generates two resonant frequency points within a single sensing area. Consequently, any environmental effect causes changes at both resonant frequency points simultaneously [37].

Existing dual-band and differential resonator designs show promising sensitivity, but still have relatively low Q-factors, such as 267.5 and 53.7 in [30], 280 and 110 in [32], 66 and 67 in [34], and 52.7 in [35]. By introducing a simultaneous yet completely independent dual-resonator architecture, the proposed design achieves a much higher Q-factor. This advancement improves frequency selectivity, enhances measurement precision, and provides more stable and reliable sensing performance than previous designs.

This paper presents a novel microwave sensor designed to overcome the limitations of mutual dependency in dual-band sensing systems by enabling isolated tuning and independent response across two operating bands. The proposed sensor consists of a pair of non-identical, symmetrically arranged, rectangle-shaped resonators, each with a distinct sensing area. Operating at resonant frequencies of $f_{r1} = 2.16$ GHz and $f_{r2} = 4.03$ GHz, it is fabricated on a Rogers 5880 substrate with $\varepsilon_r = 2.2$, $\tan\delta = 0.0009$, and a thickness of 0.79 mm. The design's independent characteristics and spatially separated sensing regions allow for the simultaneous characterization of different materials under test (MUTs). The sensor's performance has been successfully verified through both simulation and experimental validation for permittivity measurements ranging from 1 to 4.4.

2. THE THEORY OF RESONANCE PERTURBATIONS

Perturbation theory is a technique used to calculate energy changes caused by small disturbances, such as electric or magnetic fields. In microwave sensors, the permittivity of the MUT can be determined using this theory. When the MUT is placed on top of the resonator, it disturbs the resonator's electric and magnetic fields. The effective permittivity of the dielectric sample influences the capacitance and interacts with the electric field, altering the intensity of the field distribution within the sensor's structure. This can be assessed using Equation (1) [10, 26]:

$$\frac{\Delta f_r}{f_r} = \frac{\int_{v_s} (\Delta\varepsilon E_1 \cdot E_0)\, dv}{\int_{v_c} \left(\varepsilon_0 |E_0|^2\right) dv} \tag{1}$$

When a sample of dielectric material is placed on the sensor's detecting area, the change in the resonator's resonant frequency is denoted by Δf_r. The resonant frequency of the resonator without a sample is represented by f_r, the permittivity of free space by $\Delta\varepsilon$, and the change in permittivity by $\Delta\varepsilon$. Here, ε_0 refers to the electric field in the absence of the MUT sample, while E_1 represents the electric field when the MUT is placed in the region of strong field concentration within the resonator. Positioning a dielectric sample at the point of maximum electric field perturbs the field distribution, leading to a shift in the resonant frequency and a modification of the quality factor. This phenomenon enables the proposed sensor design to be used for characterizing the dielectric properties of the sample.

Fig. 1 illustrates the transmission coefficient (S_{21}) response of the sensor, comparing the scenario when the sensor is empty (red curve) with that when a material under test (MUT) is placed on it (blue curve). The observed frequency shift, Δf, signifies the interaction between the sensor's resonator and the MUT, which directly correlates with the material's permittivity. This frequency shift is fundamental for extracting the dielectric properties of different materials.

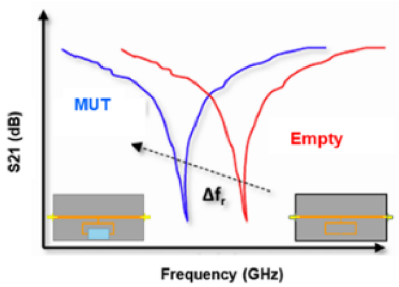

FIGURE 1. Typical response (S_{21}) of power transmission of resonator loaded and empty samples.

Referring to Equation (1), it is evident that changes in the permittivity of the MUT correspond to variations in the resonant frequency. When the MUT is placed in the sensing area, it perturbs the electric field (E-field). The resonant frequency shifts as a result of the interaction between the MUT and the resonator, which can be modeled as a capacitive load. The sensitivity of the sensor is determined by the ratio of the frequency shift to the change in the MUT's permittivity. The sensor's sensitivity (S) can be calculated using the following expression Equation (2) [38, 39]:

$$S = \frac{\Delta f}{\Delta\varepsilon_r} = \frac{(f_{Unloaded} - f_{Loaded})}{\varepsilon_{r(MUT)} - \varepsilon_{r(Reference)}} \tag{2}$$

Fig. 2 presents sensitivity analysis plots, where the sensitivity is defined as the change in frequency per unit permittivity difference ($\Delta\varepsilon_r$). The sensitivity follows a quadratic trend, represented by the equation $y = ax^2 - bx + c$, indicating that the sensor exhibits a nonlinear decreasing sensitivity trend as $\Delta\varepsilon_r$ increases, where the coefficients a, b, c can be found by using standard MUT, which suggests that the sensor performs optimally at lower permittivity values, offering higher sensitivity in this range.

According to [38], the reference permittivity that is typically utilized is that of a vacuum, with $\varepsilon_r = 1$. When being placed in the sensor's sensing area, a structure with a high electric field intensity improves coupling and field interaction with the testing sample, leading to high sensitivity. The normalized sensitivity of the sensor design can be calculated using Equation (3)

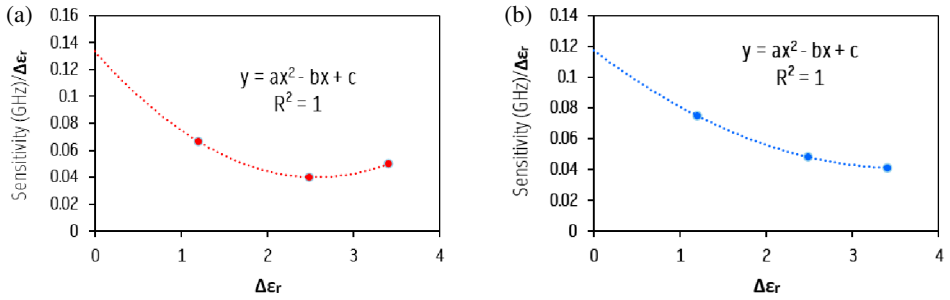

FIGURE 2. Sensitivity of proposed dual-band sensor, (a) the first resonator, (b) the second resonator.

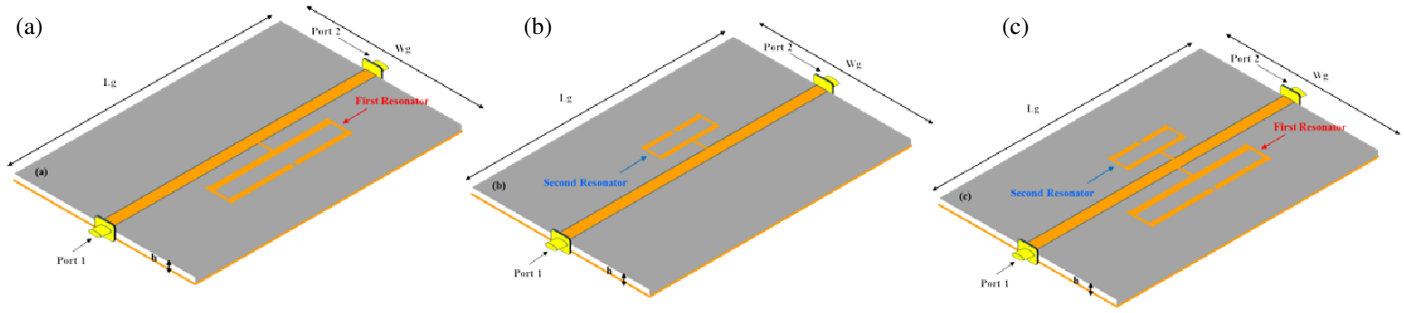

FIGURE 3. The overall design of the sensor, (a) the first resonator, (b) the second resonator, (c) dual-band resonator.

below [10, 38]:

$$NS = \frac{1}{\Delta\varepsilon_r}\left(\frac{f_{Unloaded} - f_{Loaded}}{f_{Unloaded}}\right)\% \tag{3}$$

In Equation (3), the ratio of the resonant frequency of the empty sample to that of the loaded sample in the sensing zone of the designed structure is used to determine the change in the permittivity of the tested dielectric material.

3. SIMULATION AND DESIGN OF THE PROPOSED SENSOR

3.1. Design of Proposed Sensor

A Rogers 5880 substrate with a thickness (h) of 0.79 mm, a dielectric constant ε_r of 2.2, and a loss tangent $(\tan\delta)$ of 0.0009 is used in the construction of the proposed sensor. It features a microstrip feed line with a 50 Ohm impedance and two rectangular resonators coupled by a power divider. The sensor design process is illustrated in Fig. 3.

The mathematical modeling Equation (4) is used in the sensor design, which is the standard equation for determining the dimensions of a microstrip feed line [40]. In [41], this theoretical relationship was validated through experimental analysis and variations using a microstrip ring resonator configuration. The results show that the resonance frequency shift (Δf_r) is strongly correlated with the MUT permittivity.

$$l = \frac{c}{2\sqrt{\varepsilon_{eff}}} x \frac{1}{f_r} \tag{4}$$

To determine and analyze the E-field distribution of the resonator, High Frequency Structure Simulator (HFSS) software was utilized. The simulation results illustrate the electric field distributions and frequency response of a dual-resonator microwave sensor designed for material characterization. The sensor structure consists of two resonators: the first resonator (red) and the second resonator (blue). Each resonator operates at a distinct resonant frequency, enabling dual-frequency sensing to enhance accuracy and versatility. In Fig. 4(a), the electric field distribution is highly concentrated in the sensing area of the first resonator, as indicated by the red dashed box, demonstrating strong field localization. This concentration signifies that the first resonator is dominant at its operating frequency, making it highly sensitive to the perturbations caused by a material under test (MUT). In Fig. 4(b), the field distribution shifts toward the second resonator's sensing area, highlighted by the blue dashed box, showing its sensitivity to material perturbations at its respective resonance frequency, thereby enabling a complementary frequency response. This dual-resonator design improves the sensor's performance by providing two independent sensing frequencies, increasing measurement reliability and extending the sensing range. Fig. 4(c) presents the sensor's frequency response (S_{21} parameter), representing the transmission coefficient. The simulation results validate the sensor's effectiveness, demonstrating its capability to operate at two distinct frequencies with localized electric fields, ensuring accurate and independent material characterization.

The resonator operates at frequencies ranging from 1 GHz to 6 GHz. The suggested sensor measures 54 mm × 25 mm × 0.79 mm, and Figs. 5(a) and (b) show the design structure. As illustrated in Fig. 5(c), the sensor uses a two-port arrangement with SMA connectors and an impedance of $Z_0 = 50$ ohms. Figure 4(d) shows equivalent circuit, and Fig. 5(e) presents a comparison of the S_{21} parameters, demonstrating that the experimental results show good agreement between the element

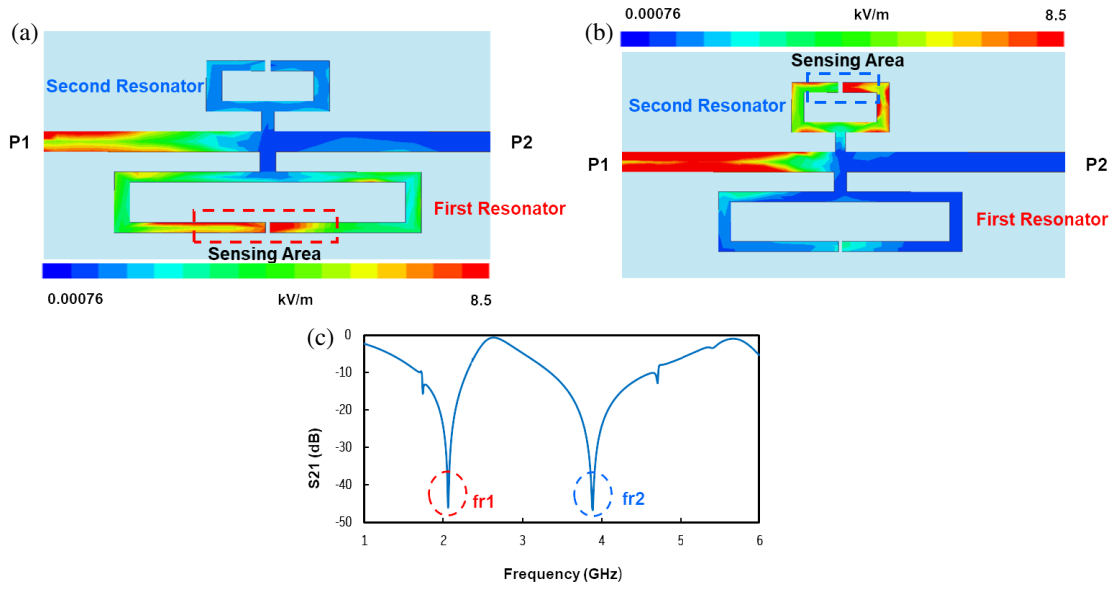

FIGURE 4. (a) Sensing area at first resonator, (b) sensing area at second resonator, (c) S_{21} parameters behaviour of proposed resonator.

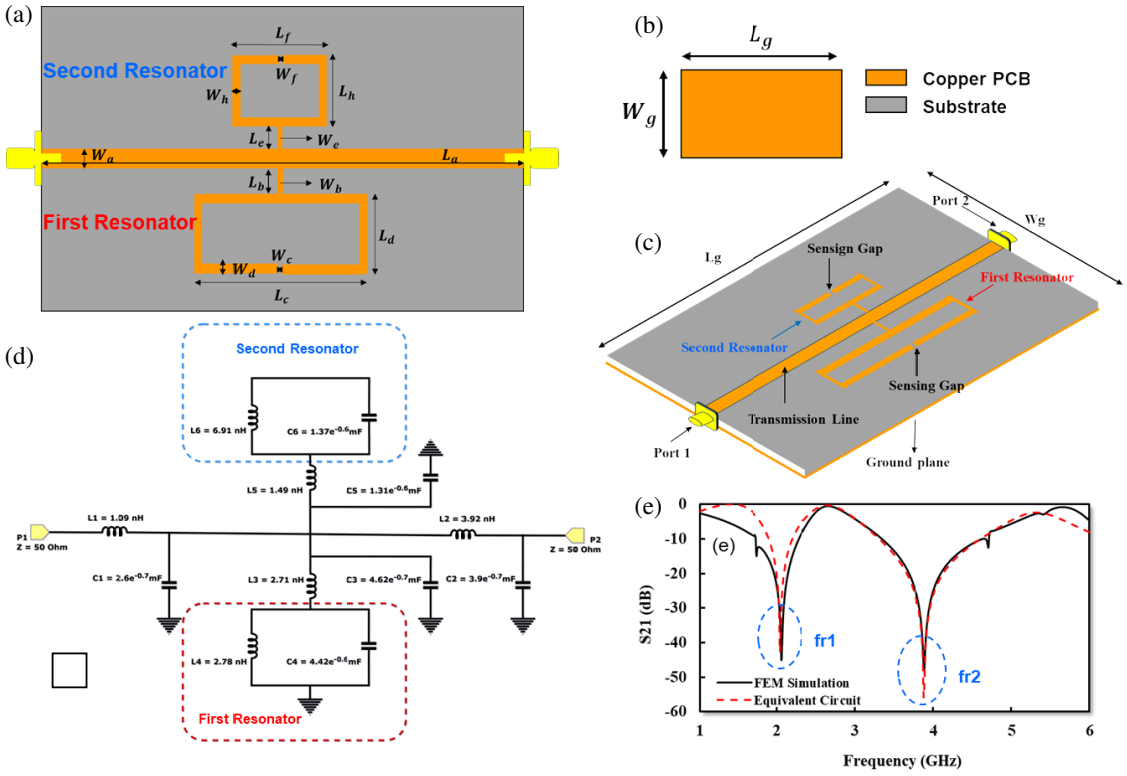

FIGURE 5. Design of proposed sensor, (a) front view, (b) back view, (c) perspective view, (d) equivalent circuit, (e) along with a comparison of S_{21} between the element model and full-wave EM simulation.

model and full-wave EM simulation. The overall optimized dimensions of the dual-band sensor with rectangle-shaped resonators are summarized in Table 1.

3.2. Location of Material Under Test (MUT)

In Fig. 6(a), the fabricated sensor is displayed. Each resonator has a unique sensing area with a strong E-field, as indicated by the results of HFSS simulations. Strong E-fields are observed in the first resonator at $f_{r1} = 2.06$ GHz and $f_{r2} = 3.89$ GHz. Based on measurement results, the resonant frequencies obtained are $f_{r1} = 2.16$ GHz and $f_{r2} = 4.03$ GHz for each resonator. A comparison of the proposed sensor's simulation and measurement results is shown in Fig. 6(b). It is evident that the dual-band features in the simulation and measurement data are identical. However, for each resonant frequency, there were

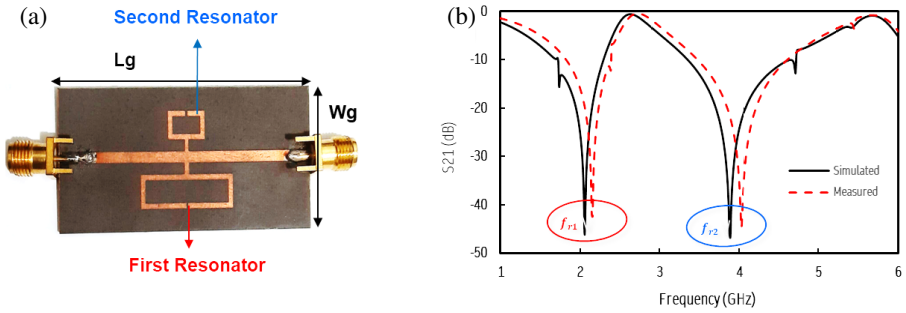

FIGURE 6. (a) Fabricated, proposed microwave resonator, (b) simulation and measurement of the proposed resonator.

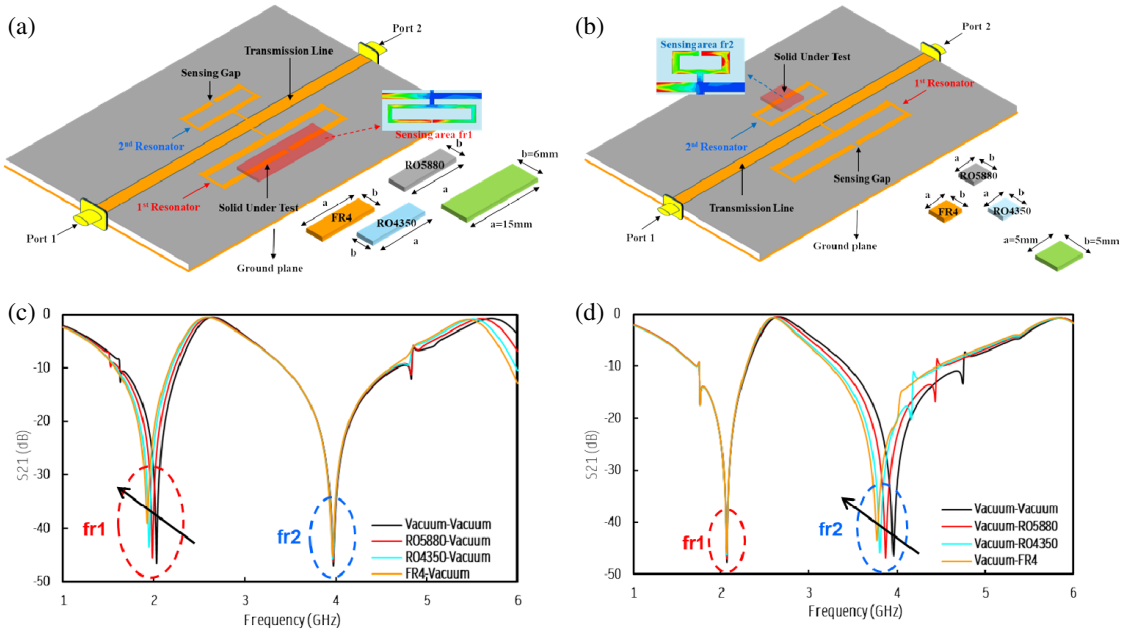

FIGURE 7. (a) Placement MUT in first resonator, (b) placement MUT in second resonator, (c) S_{21} parameters behaviour with MUT in first resonator, (d) S_{21} parameters behaviour with MUT in second resonator.

TABLE 1. Dimensions of rectangle-shaped resonators.

Parameter	Value	Parameter	Value
L_g	54 mm	W_g	25 mm
L_a	54 mm	W_a	2 mm
L_b	2 mm	W_b	1 mm
L_c	20 mm	W_c	0.3 mm
L_d	6 mm	W_d	1 mm
L_e	2 mm	W_e	0.8 mm
L_f	8 mm	W_f	0.4 mm
L_h	5 mm	W_h	1 mm

frequency shifts of 4.63% and 3.47% between the modeling and measurement results, which were likely caused by fabrication defects.

The material under test (MUT) was placed on one of the resonators to perform the test. As MUTs, three conventional material types RO5880, RO4350B, and FR4 with known permittivity were employed. RO5880 has a thickness of 3.18 mm, a permittivity of 2.2, and a loss tangent ($\tan\delta$) of 0.0009. RO4350B has a thickness of 0.51 mm, a permittivity of 3.48, and a loss tangent ($\tan\delta$) of 0.004, whereas FR4 has a thickness of 1.6 mm, a permittivity of 4.4, and a loss tangent ($\tan\delta$) of 0.03.

Figures 7(a) and 7(b) illustrate the microwave sensor configurations, emphasizing the MUT placement in two distinct sensing areas corresponding to the two resonators. These configurations facilitate a comparative analysis of the sensor's response to different dielectric materials under identical excitation conditions. Figs. 7(c) and 7(d) depict the simulated scattering parameter (S_{21}) responses for various MUT scenarios across a frequency range of 1 GHz to 6 GHz. A noticeable frequency shift occurs for each material, reflecting the relationship between the material's dielectric constant and resonant frequency. This result highlights the sensor's capability to differentiate materials based on their dielectric properties.

The results presented in Fig. 8 illustrate the variation of resonant frequencies f_{r1} and f_{r2} as a function of the dielectric permittivity (ε_r) of the MUT. Figs. 8(a) and 8(b) depict the distinct responses of two independent resonators in the microwave sensor when different materials are placed in the sensing region. In Fig. 8(a), the first resonant frequency (f_{r1}) exhibits

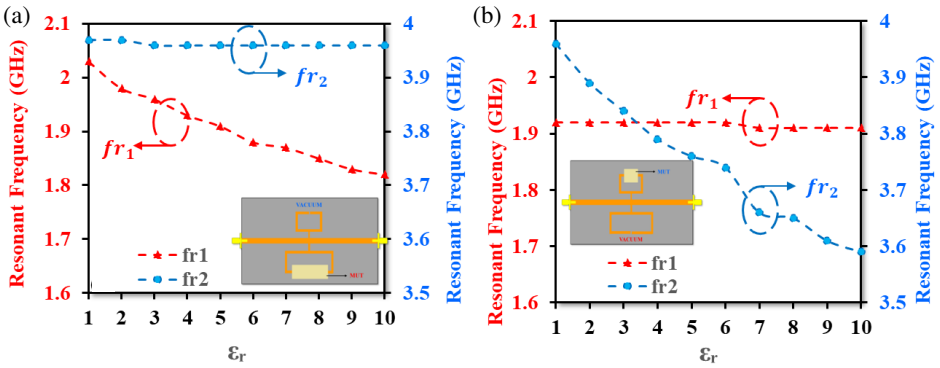

FIGURE 8. Correlation of f_{r1} and f_{r2} when the MUT is loaded on (a) the first resonator, (b) the second resonator.

a clear downward trend from 2.03 GHz to 1.82 GHz as ε_r increases, indicating a strong dependence on the permittivity of the MUT. This behavior aligns with theoretical expectations, as materials with higher permittivity tend to lower the effective resonant frequency due to increased capacitance. In contrast, the second resonant frequency (f_{r2}) remains relatively stable, with only minor fluctuations between 3.96 GHz and 3.97 GHz, suggesting that the first resonator is primarily responsible for sensing changes in ε_r at lower frequencies. Fig. 8(b) presents a complementary scenario, where f_{r2} experiences a significant decrease from 3.96 GHz to 3.59 GHz with increasing ε_r, while f_{r1} shifted but not significantly between 1.91 GHz and 1.92 GHz. It indicates that the second resonator is more sensitive to permittivity variations in a different frequency band. The observed trends confirm the independent operation of the two resonators, allowing simultaneous characterization of multiple materials. By analyzing the difference between the resonant frequencies corresponding to the lowest and highest permittivities of the MUT, the simulation results show that the first and second resonators exhibit a Δf of 0.21 GHz and 0.37 GHz, respectively. Overall, the results confirm that the sensor can independently and accurately characterize dielectric materials. The distinct frequency shifts of f_{r1} and f_{r2} enable dual-band operation, making the sensor suitable for applications requiring precise permittivity measurements across different frequency ranges.

Based on Fig. 9, the results illustrate the performance of a dual-resonator microwave sensor for material characterization. The sensor consists of two non-identical rectangular resonators, enabling independent and simultaneous detection of solid materials. The experimental setup, as shown in the diagrams, involves different dielectric materials, including RO5880, RO4350, and FR4, placed on the sensing areas of the resonators. The corresponding S-parameter (S_{21}) responses reveal shifts in resonant frequencies, indicating the sensor's sensitivity to the dielectric permittivity (ε_r) of the materials under test (MUTs).

In the frequency response graphs, two resonant frequencies, f_{r1} and f_{r2}, are observed, each corresponding to one of the resonators. The shifts in f_{r1} and f_{r2} with different materials confirm the impact of the MUT's permittivity. The black curve represents the baseline measurement in a vacuum, while the colored curves correspond to different MUTs. The resonant frequency decreases as the permittivity increases, confirming the sensor's ability to differentiate materials based on their dielectric properties. Notably, FR4 exhibits the most significant frequency shift due to its higher permittivity, while RO5880 shows minimal deviation as its permittivity closely matches the substrate.

Additionally, the sensor demonstrates a distinct advantage by enabling independent measurements at different resonators, allowing for simultaneous material characterization. The experimental results validate the effectiveness of the sensor in accurately detecting changes in permittivity while maintaining a high Q-factor. This makes the proposed sensor suitable for applications in material quality control, biomedical diagnostics, and industrial testing. Future work may explore further optimizations to enhance sensitivity and broaden the range of measurable permittivity values.

4. MEASUREMENT AND VERIFICATION

4.1. Measurements of Proposed Sensors

Figure 10 illustrates the experimental setup and measurement results of a dual-resonator microwave sensor for material characterization. Fig. 10(a) shows the system, comprising a vector network analyzer (VNA) connected to the sensor via coaxial cables. The MUT includes RO5880, RO4350B, and FR4, each with a distinct dielectric constant. Two scenarios are analyzed, Scenario 1 (MUT placed over f_{r2}) and Scenario 2 (MUT placed over f_{r1}). In Scenario 1 (Fig. 10(b)), f_{r1} remains unaffected at 2.16 GHz since the MUT is outside its sensing region. For RO5880 and RO4350, the second resonator's resonance frequency (f_{r2}) $=$ 4.03 GHz shifted to 3.94 GHz and 3.91 GHz, respectively, whereas for FR4, it shifts to 3.89 GHz. Conversely, in Scenario 2 (Fig. 10(c)), f_{r2} remains stable at 4.03 GHz. The resonant frequency of the 1st resonator (f_{r1}) shifts from 2.16 GHz to 2.08 GHz for RO5880, 2.06 GHz for RO4350, and for FR4 to 1.99 GHz. These results confirm the sensor's ability to independently characterize materials by detecting shifts in resonance dips. The sensor effectively distinguishes dielectric materials based on permittivity, leveraging dual-resonance operation for enhanced accuracy and multi-frequency sensing. The measured data align well with simulations, demonstrating that f_{r1} and f_{r2} operate independently and remain highly sensitive to permittivity variations.

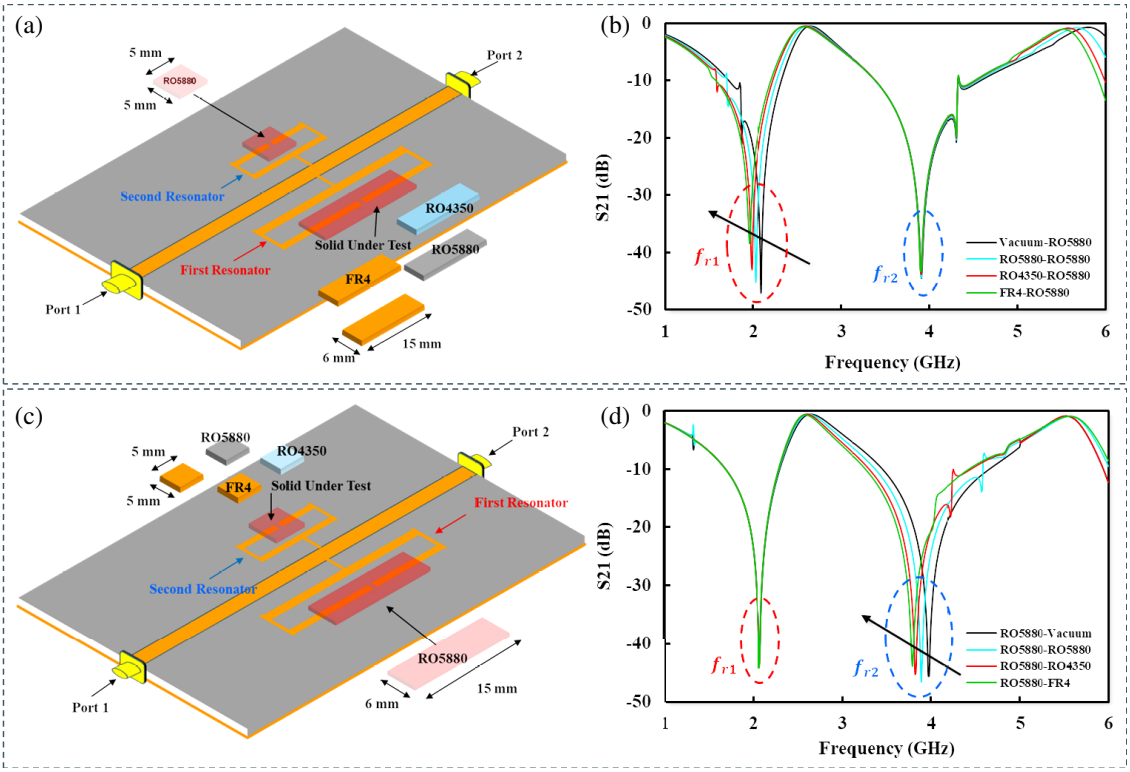

FIGURE 9. (a) Placement of material under test and shift frequency of the first resonator with the second resonator as RO5880, (b) placement material under test and shift frequency of the second resonator with the first resonator as RO5880.

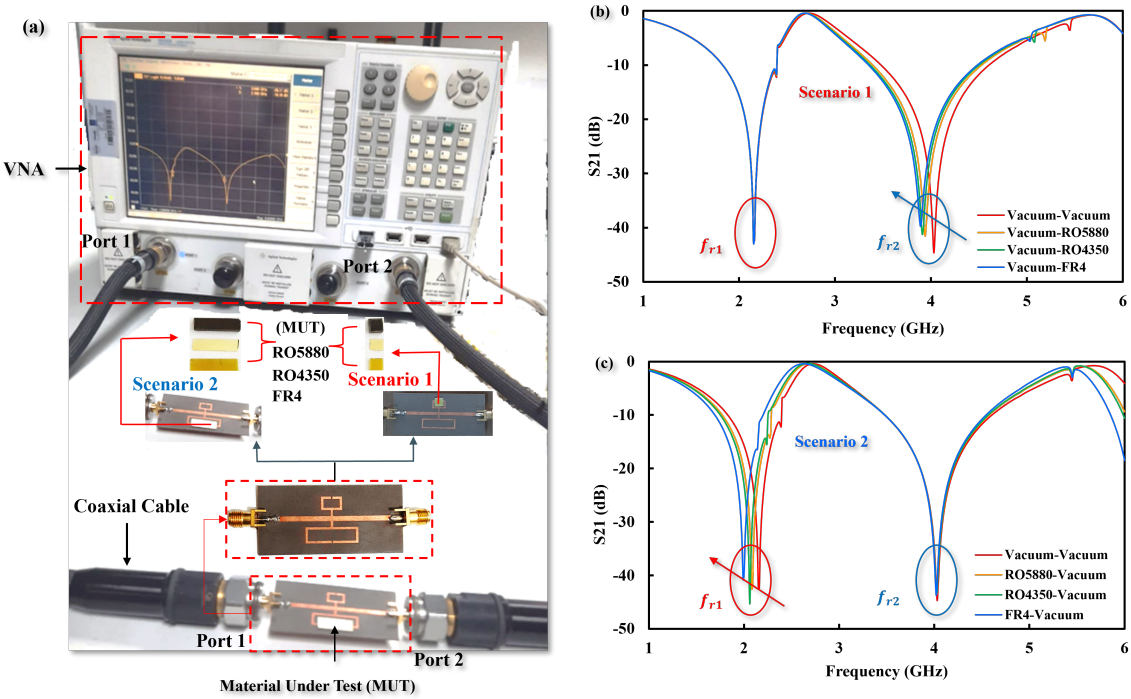

FIGURE 10. (a) Measurement of proposed resonator, (b) correlation of f_{r1} and f_{r2} when the MUT is loaded on the second resonator with the first resonator as vacuum, (c) correlation of f_{r1} and f_{r2} when the MUT is loaded on the first resonator with the second resonator as vacuum.

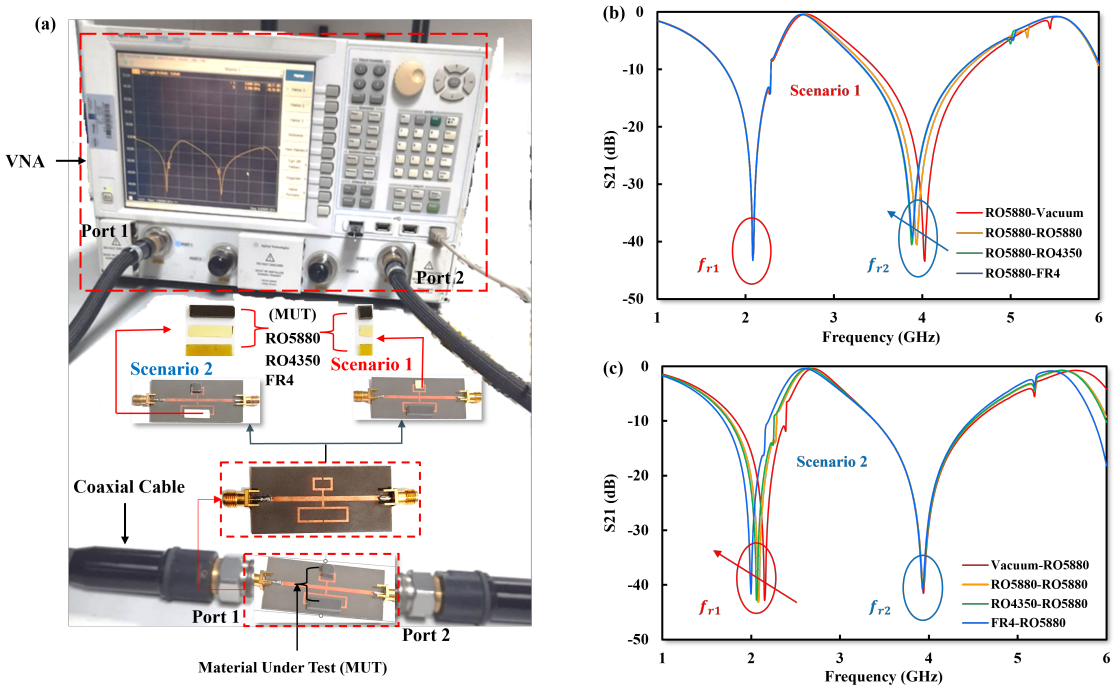

FIGURE 11. (a) Measurement of the proposed resonator, (b) correlation of f_{r1} and f_{r2} when the MUT is loaded on the second resonator with the first resonator as RO5880, (c) correlation of f_{r1} and f_{r2} when the MUT is loaded on the first resonator with the second resonator as RO5880.

TABLE 2. Overall summary of experimental results for the first resonator with MUT (the second resonator as vacuum).

MUT	ε_r (Ref)	Size of MUT (mm^3)	Resonance Frequency f_{r1} (GHz)	Δf	$\Delta\varepsilon_r$	Sensitivity $S = \Delta f/\Delta\varepsilon_r$ (GHz)	Measured Permittivity (ε_r)	Q-factor	% Error	% Accuracy	NS (%)
Vacuum	1	-	2.16	0	0	-	0.95	308	4.51	95.49	-
RO5880	2.2	$16 \times 5 \times 3.18$	2.08	0.08	1.2	0.067	2.63	231	19.48	80.52	3.09
RO4350	3.48	$16 \times 5 \times 0.51$	2.06	0.1	2.48	0.04	3.04	226	12.65	87.35	1.87
FR4	4.4	$16 \times 5 \times 1.60$	1.99	0.17	3.4	0.05	4.46	86	1.32	98.68	2.31

In Fig. 11, testing was conducted by simultaneously placing the MUT on both resonators. Various materials, including RO5880, RO4350, and FR4, were placed on one resonator to evaluate their effect on the resonant frequency, while RO5880 was placed on the other resonator. Figs. 11(b) and (c) show the S-parameter (S_{21}) responses under two testing scenarios. In Scenario 1 (Fig. 11(b)), f_{r1} shifts while f_{r2} remains stable, indicating that the MUT primarily affects the first resonator. In Scenario 2 (Fig. 11(c)), f_{r2} shifts while f_{r1} remains unchanged, demonstrating independent sensing by the second resonator. Frequency shifts correlate with the dielectric permittivity (ε_r), where higher permittivity materials cause a greater downward shift. These results confirm the sensor's effectiveness in dual-band, independent material characterization. Its ability to measure two materials simultaneously with minimal cross-interference makes it valuable for applications in material quality control, biomedical diagnostics, and industrial sensing. Future work may enhance sensitivity, expand the measurable permittivity range, and explore additional applications.

4.2. Verification of Measurement Result

Furthermore, a mathematical model was used using a curve-fitting technique to validate the measurement results. The permittivity of unknown materials is extracted using the fitted equation. Tables 2 and 3 provide a detailed analysis of dielectric permittivity measurements conducted using a microwave sensor under various conditions and MUT configurations.

The measured permittivity for vacuum closely aligns with the expected value, demonstrating high accuracy. Meanwhile, materials such as RO5880, RO4350, and FR4 exhibit frequency shifts of 0.09 GHz, 0.12 GHz, and 0.14 GHz, respectively, when the 2nd resonator is loaded, and frequency shifts of 0.08 GHz, 0.1 GHz, and 0.17 GHz, respectively, when the 1st resonator is loaded. These shifts correlate with their respective permittivity values of 2.2, 3.48, and 4.4. It can be seen that f_{r1} and f_{r2} achieve average accuracies of 90.51% and 95.16%, respectively, while the normalized sensitivities of the two resonators reach 2.42% and 1.36%, respectively. In addition, the Q-factors of resonators are 308 and 537, respectively.

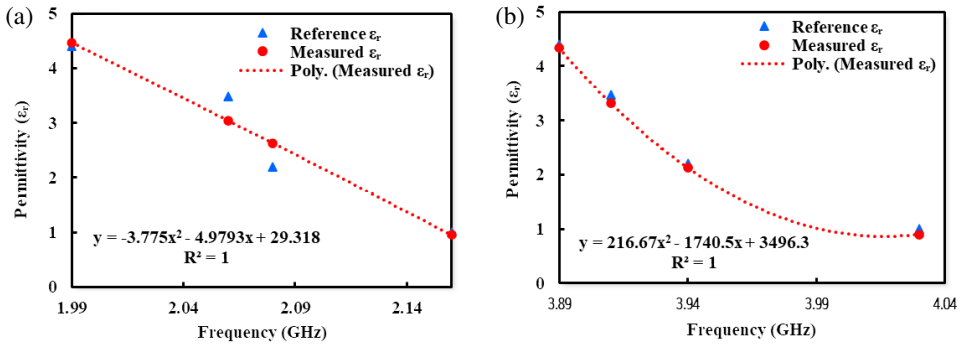

FIGURE 12. The fitting curve of the material under test (MUT) from the measurement is compared with the reference for (a) the first resonator and (b) the second resonator.

TABLE 3. Overall summary of experimental results for the second resonator with MUT (first resonator as vacuum).

MUT	ε_r (Ref)	Size of MUT (mm^3)	Resonance Frequency f_{r2} (GHz)	Δf	$\Delta\varepsilon_r$	Sensitivity $S = \Delta f/\Delta\varepsilon_r$ (GHz)	Measured Permittivity (ε_r)	Q-factor	% Error	% Accuracy	NS (%)
Vacuum	1	-	4.03	0	0	-	0.90	537	10.26	89.74	-
RO5880	2.2	$5 \times 5 \times 3.18$	3.94	0.09	1.20	0.075	2.13	315	3.06	96.94	1.86
RO4350	3.48	$5 \times 5 \times 0.51$	3.91	0.12	2.48	0.048	3.32	261	4.52	95.48	1.20
FR4	4.4	$5 \times 5 \times 1.60$	3.89	0.14	3.40	0.041	4.33	195	1.54	98.46	1.02

TABLE 4. Overall summary of experimental results for both resonators with MUT (second resonator as RO5880).

MUT	ε_r (Ref)	Size of MUT (mm^3)	Resonance Frequency f_{r1} (GHz)	Δf	$\Delta\varepsilon_r$	Sensitivity $S = \Delta f/\Delta\varepsilon_r$ (GHz)	Measured Permittivity (ε_r)	Q-factor	% Error	% Accuracy	NS (%)
Vacuum	1	-	2.15	0	0	-	0.95	307	4.79	95.21	-
RO5880	2.2	$16 \times 5 \times 3.18$	2.08	0.07	1.20	0.058	2.59	277	18.09	81.91	2.71
RO4350	3.48	$16 \times 5 \times 0.51$	2.06	0.09	2.48	0.036	3.06	257	11.90	88.10	1.69
FR4	4.4	$16 \times 5 \times 1.60$	2.00	0.15	3.40	0.044	4.46	222	1.39	98.61	2.05

TABLE 5. Overall summary of experimental results for both resonators with MUT (first resonator as RO5880)).

MUT	ε_r (Ref)	Size of MUT (mm^3)	Resonance Frequency f_{r2} (GHz)	Δf	$\Delta\varepsilon_r$	Sensitivity $S = \Delta f/\Delta\varepsilon_r$ (GHz)	Measured Permittivity (ε_r)	Q-factor	% Error	% Accuracy	NS (%)
Vacuum	1	-	4.03	0	0	-	1.01	350	1.21	98.79	-
RO5880	2.2	$5 \times 5 \times 3.18$	3.94	0.09	1.20	0.075	2.42	246	9.87	90.13	1.86
RO4350	3.48	$5 \times 5 \times 0.51$	3.88	0.15	2.48	0.060	4.06	228	16.56	83.44	1.50
FR4	4.4	$5 \times 5 \times 1.60$	3.89	0.14	3.40	0.041	3.74	222	14.91	85.09	1.02

In Tables 4 and 5, the MUT is placed on both resonators simultaneously. Various materials, including RO5880, RO4350, and FR4, are placed on one resonator, while RO5880 is placed on the other. The results obtained for f_{r1} and f_{r2} achieve average accuracies of 90.96% and 89.36%, respectively. The normalized sensitivities are 2.15% and 1.46%, while the Q-factors of the resonators are 307 and 350, respectively.

Figs. 12(a) and 12(b) present the measured and reference permittivity (ε_r) values as a function of frequency for two different frequency bands, highlighting the performance of the microwave sensor for material characterization. In Fig. 12(a), the measured permittivity values (ε_r) are represented by red circular markers and fitted using a second-order polynomial regres-

TABLE 6. The sensitivity results following the quadratic trend.

MUT	First Resonator loaded		Second resonator loaded	
	x	y	x	y
	$\Delta\varepsilon_r$	S	$\Delta\varepsilon_r$	S
RO5880	1.2	0.067	1.2	0.075
RO4350	2.48	0.040	2.48	0.048
FR4	3.4	0.050	3.4	0.041

TABLE 7. Comparison of proposed sensor based on previous literature.

Ref.	Method	Range of Permittivity (ε_r)	Resonance Frequency (GHz)		Q-factor	Material Under Test (MUT)	Accuracy %		NS %	No. of Sensing	Dual-Band	Independence Performance
			f_{r1}	f_{r2}			f_{r1}	f_{r2}				
[19]	CSRR	1–4.4	2.5	-	520	Solid	-	-	-	1	No	NA
[21]	CSRR & Nested CSRR	1–4	3.37	-	464	Solid	94.25	-	3.48	1	No	NA
[26]	Microwave sensor Non-Contact	3–6	1.38	-	-	Solid	97 and 92	-	0.51	1	No	NA
[29]	CSSSR	2.1–3	15.12	-	-	Solid	-	-	6.7	1	No	NA
[42]	Compact maze-shaped meta	1–10	2.77 and 3.08	-	-	Solid	-	-	11.91 and 12.01	1	No	NA
[30]	CSSRR	1–12	5.35	7.99	267.5 and 53.7	Solid	-	-	9.7	2	YES	No
[32]	SRR	24–78	5.76	7.85	280 and 110	Liquid	99.02	94.63	0.28 and 0.3	2	YES	No
[34]	HSRR	1–20.6	5.3	-	66.67	Liquid	98.8	-	4.646	2	YES	No
[35]	IDC-SRRs	2–14	4.15	9.18	52.7	Liquid	-	-	0.87 and 0.61	2	YES	No
[36]	SRR and Coupled L Resonators	1–80	2.234	1.634 and 1.819	-	Solid Liquid	-	-	0.073 and 0.06	2	YES	YES
[37]	E-Interdigital Structure	1–3	3 and 3.92	-	-	Solid	-	-	-	2	YES	YES
This Work	Dual Rectangular-Shape	1–4.4	2.16	4.03	308 and 537	Solid	98.68	98.79	1.69 and 1.02	2	YES	YES

sion, depicted by a dotted red line.

$$\varepsilon_r\left(fr_1\right) = -3.775f^2 - 4.9793f + 29.318 \quad (5)$$

where f is the frequency in GHz. The reference permittivity values, indicated by blue triangular markers, provide a baseline for comparison. The measured data closely follow the reference trend, demonstrating the sensor's reliability and accuracy within the frequency range of 1.99 to 2.16 GHz. The decreasing trend in permittivity with increasing frequency is consistent with the dispersive behavior of materials in this band. Similarly, Fig. 12(b) presents the results for a higher frequency band (3.89 to 4.03 GHz). Here, the measured values are represented by red circular markers.

$$\varepsilon_r\left(fr_2\right) = 216.67f^2 - 1740.5f + 3496.3 \quad (6)$$

The strong agreement between measured and reference permittivity values reaffirms the sensor's capability to characterize materials across multiple frequency bands. The sharper decline in permittivity at higher frequencies, as shown in the graph, further emphasizes the frequency-dependent nature of dielectric properties.

Furthermore, Figs. 13(a) and 13(b) illustrate the sensitivities of the first and second resonators. The maximum sensitivities of the two resonators are 0.067 GHz/$\Delta\varepsilon_r$ and 0.075 GHz/$\Delta\varepsilon_r$, respectively, as determined using Equation (2). The sensitivity results following the quadratic trend are presented in Table 6. Meanwhile, the maximum normalized sensitivities of the first and second resonators are 3.08 and 1.86, respectively, obtained using Equation (3). Meanwhile, the maximum normalized sen-

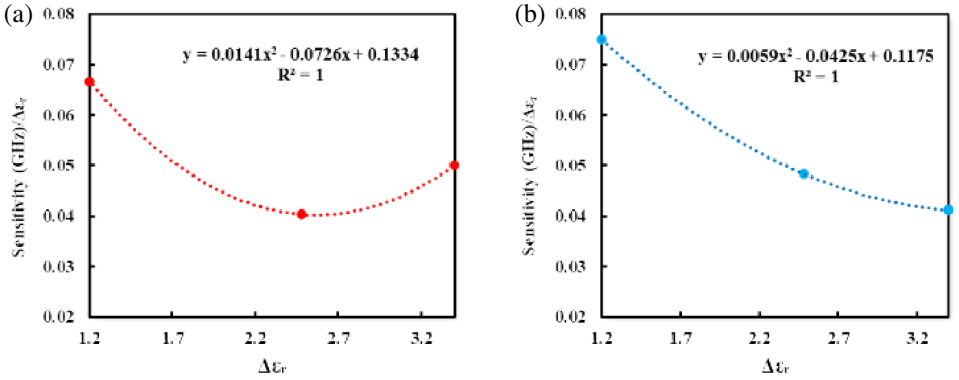

FIGURE 13. Prediction value of sensitivity with $\Delta\varepsilon_r$, (a) the first resonator, (b) the second resonator.

sitivities of the first and second resonators are 3.08 and 1.86, respectively, obtained using Equation (3).

5. EXPERIMENTAL VALIDATION WITH EXISTING SENSOR

Based on the simulation and measurement results, two rectangular resonators with separate sensing areas can be used to assess the permittivity of several MUTs simultaneously and independently. Table 7 compares the proposed sensor with previously developed sensors, evaluating parameters such as models, number of sensing areas, number of ports, MUT type, Q-factor, accuracy, and normalized sensitivity. The proposed sensor, as depicted in Table 7, enables the independent detection of two different types of MUTs at separate sensing areas.

This study introduces a novel approach to measuring the permittivity of MUTs independently, leveraging the rectangle-shaped resonator design to generate distinct sensing regions. In the future, this sensor could be adapted to simultaneously detect both solid and liquid MUTs, utilizing each resonator according to its independent characteristics.

Therefore, further investigations are recommended to assess the sensor's performance in permittivity measurements for different MUTs under simultaneous testing.

6. CONCLUSION

This study successfully presents a dual-band independent permittivity sensor employing a two-port design with a pair of rectangle-shaped resonators for simultaneous and independent solid material detection. It operates at resonant frequencies of $f_{r1} = 2.16$ GHz and $f_{r2} = 4.03$ GHz. The rectangular resonators are symmetrically arranged to create distinct sensing areas, enabling the independent placement of two materials. The advantage of the suggested sensor is that it can independently and simultaneously measure the permittivity of the material under test (MUT) at two distinct sensing points with high accuracy. The measurement results indicate that f_{r1} and f_{r2} achieve average accuracies of 98.68% and 98.79%, respectively, for a permittivity range of 1–4.4, while the normalized sensitivities are 1.69% and 1.02%. In addition, the Q-factors of resonators are 308 and 537, respectively. Therefore, the proposed sensor has potential applications in the food industry, material quality control, and biomedical fields.

REFERENCES

[1] Navaei, M., P. Rezaei, and S. Kiani, "Microwave split ring resonator sensor for determination of the fluids permittivity with measurement of human milk samples," *Radio Science*, Vol. 57, No. 7, 1–11, Jul. 2022.

[2] Alahnomi, R. A., Z. Zakaria, M. A. M. Said, Z. M. Yussof, A. Alhegazi, H. Alsariera, and N. A. Rahman, "Enhanced T-resonator with blazed grating for accurate powder material characterization," in *2020 IEEE International RF and Microwave Conference (RFM)*, 1–4, Kuala Lumpur, Malaysia, Dec. 2020.

[3] Al-Gburi, A. J. A., Z. Zakaria, I. M. Ibrahim, R. S. Aswir, and S. Alam, "Solid characterization utilizing planar microwave resonator sensor," *Applied Computational Electromagnetics Society Journal (ACES)*, Vol. 37, No. 2, 222–228, Feb. 2022.

[4] Al-Gburi, A. J. A., Z. Zakaria, N. A. Rahman, A. A. Althuwayb, I. M. Ibrahim, T. Saeidi, Z. A. Dayo, and S. Ahmad, "A miniaturized and highly sensitive microwave sensor based on CSRR for characterization of liquid materials," *Materials*, Vol. 16, No. 9, 3416, 2023.

[5] Buragohain, A., A. T. T. Mostako, and G. S. Das, "Low-cost CSRR based sensor for determination of dielectric constant of liquid samples," *IEEE Sensors Journal*, Vol. 21, No. 24, 27 450–27 457, Dec. 2021.

[6] Gulsu, M. S., F. Bagci, S. Can, A. E. Yilmaz, and B. Akaoglu, "Minkowski-like fractal resonator-based dielectric sensor for estimating the complex permittivity of binary mixtures of ethanol, methanol and water," *Sensors and Actuators A: Physical*, Vol. 330, 112841, 2021.

[7] Wu, W.-J., W.-S. Zhao, and W. Wang, "A microwave sensing system combination of interdigital structure (IDS)-based microstrip line and RF circuits for extracting complex permittivity of liquid samples," *Sensors and Actuators A: Physical*, Vol. 378, 115860, Nov. 2024.

[8] Amer, R. A. B., M. A. M. Said, M. S. M. Ghani, M. H. Misran, M. A. Othman, S. Suhaimi, and N. I. Hassan, "High responsive microwave resonator sensor for material characterization," *International Journal of Academic Research in Business and Social Sciences*, Vol. 14, No. 10, 552–564, 2024.

[9] Morales-Lovera, H.-N., J.-L. Olvera-Cervantes, A.-E. Perez-Ramos, A. Corona-Chavez, and C. E. Saavedra, "Microstrip sensor and methodology for the determination of complex

anisotropic permittivity using perturbation techniques," *Scientific Reports*, Vol. 12, No. 1, 2205, 2022.

[10] Wang, C., L. Ali, F.-Y. Meng, K. K. Adhikari, Z. L. Zhou, Y. C. Wei, D. Q. Zou, and H. Yu, "High-accuracy complex permittivity characterization of solid materials using parallel interdigital capacitor-based planar microwave sensor," *IEEE Sensors Journal*, Vol. 21, No. 5, 6083–6093, Mar. 2021.

[11] Mohammadi, P., A. Mohammadi, and A. Kara, "Enhanced half-mode SIW loaded with interdigital capacitor for permittivity measurements," *IEEE Transactions on Instrumentation and Measurement*, Vol. 72, 1–8, 2023.

[12] Liu, Q., H. Deng, P. Meng, and H. Sun, "High sensitivity sensor loaded with octagonal spiral resonators for retrieval of solid material permittivity," *IEEE Sensors Journal*, Vol. 21, No. 18, 20 010–20 017, Sep. 2021.

[13] S, A., S. K. Menon, M. Donelli, and M. L, "Development of a microwave sensor for solid and liquid substances based on closed loop resonator," *Sensors*, Vol. 21, No. 24, 8506, 2021.

[14] Yang, L., H. Kou, X. Wang, X. Zhang, Z. Shang, J. Shi, G. Zhang, and Z. Gui, "A microwave pressure sensor loaded with complementary split ring resonator for high-temperature applications," *Micromachines*, Vol. 14, No. 3, 635, Mar. 2023.

[15] Acevedo-Osorio, G., E. Reyes-Vera, and H. Lobato-Morales, "Dual-band microstrip resonant sensor for dielectric measurement of liquid materials," *IEEE Sensors Journal*, Vol. 20, No. 22, 13 371–13 378, Nov. 2020.

[16] Al-Gburi, A. J. A., N. A. Rahman, Z. Zakaria, and M. F. Akbar, "Realizing the high Q-factor of a CSIW microwave resonator based on an MDGS for semisolid material characterization," *Micromachines*, Vol. 14, No. 5, 922, 2023.

[17] Bagci, F., M. S. Gulsu, and B. Akaoglu, "Dual-band measurement of complex permittivity in a microwave waveguide with a flexible, thin and sensitive metamaterial-based sensor," *Sensors and Actuators A: Physical*, Vol. 338, 113480, May 2022.

[18] Muñoz-Enano, J., P. Vélez, M. Gil, and F. Martín, "Planar microwave resonant sensors: A review and recent developments," *Applied Sciences*, Vol. 10, No. 7, 2615, Apr. 2020.

[19] Al-Gburi, A. J. A., Z. Zakaria, N. A. Rahman, S. Alam, and M. A. M. Said, "A compact and low-profile curve-feed complementary split-ring resonator microwave sensor for solid material detection," *Micromachines*, Vol. 14, No. 2, 384, Feb. 2023.

[20] Jang, C., J.-K. Park, H.-J. Lee, G.-H. Yun, and J.-G. Yook, "Temperature-corrected fluidic glucose sensor based on microwave resonator," *Sensors*, Vol. 18, No. 11, 3850, Nov. 2018.

[21] Abd Rahman, N., Z. Zakaria, R. A. Rahim, M. A. M. Said, A. A. M. Bahar, R. A. Alahnomi, and A. Alhegazi, "High quality factor using nested complementary split ring resonator for dielectric properties of solids sample," *Applied Computational Electromagnetics Society Journal (ACES)*, Vol. 35, No. 10, 1222–1227, Oct. 2020.

[22] Oliveira, J. G. D., E. N. M. G. Pinto, V. P. S. Neto, and A. G. D'Assunção, "CSRR-based microwave sensor for dielectric materials characterization applied to soil water content determination," *Sensors*, Vol. 20, No. 1, 255, Jan. 2020.

[23] Vélez, P., J. Muñoz-Enano, A. Ebrahimi, C. Herrojo, F. Paredes, J. Scott, K. Ghorbani, and F. Martín, "Single-frequency amplitude-modulation sensor for dielectric characterization of solids and microfluidics," *IEEE Sensors Journal*, Vol. 21, No. 10, 12 189–12 201, 2021.

[24] Said, M. A. M., Z. Zakaria, M. H. Misran, M. A. B. Othman, R. A. Manap, A. S. B. Jaafar, S. Suhaimi, and N. I. Hassan, "Planar microwave sensor with high sensitivity for material characterization based on square split ring resonator (SSRR) for solid and liquid," *EMITTER International Journal of Engineering Technology*, Vol. 11, No. 1, 60–75, 2023.

[25] Zidane, M. A., A. Rouane, C. Hamouda, and H. Amar, "Hypersensitive microwave sensor based on split ring resonator (SRR) for glucose measurement in water," *Sensors and Actuators A: Physical*, Vol. 321, 112601, Apr. 2021.

[26] Ali, L., C. Wang, I. Ullah, A. Yousaf, W. U. Khan, S. Ullah, R. Khan, F. Alassery, H. Hamam, and M. Shafiq, "Design and optimization of microwave sensor for the non-contact measurement of pure dielectric materials," *Electronics*, Vol. 10, No. 24, 3057, Dec. 2021.

[27] Soltan, A., R. A. Sadeghzadeh, and S. Mohammad-Ali-Nezhad, "Microwave sensor for liquid classification and permittivity estimation of dielectric materials," *Sensors and Actuators A: Physical*, Vol. 336, 113397, Apr. 2022.

[28] Xie, J., J. Wen, J. Chen, and W. Yuan, "Microwave icing sensor based on interdigital-complementary split-ring resonator," *IEEE Sensors Journal*, Vol. 22, No. 13, 12 829–12 837, 2022.

[29] Haq, T., C. Ruan, X. Zhang, S. Ullah, A. K. Fahad, and W. He, "Extremely sensitive microwave sensor for evaluation of dielectric characteristics of low-permittivity materials," *Sensors*, Vol. 20, No. 7, 1916, Mar. 2020.

[30] Armghan, A., T. M. Alanazi, A. Altaf, and T. Haq, "Characterization of dielectric substrates using dual band microwave sensor," *IEEE Access*, Vol. 9, 62 779–62 787, 2021.

[31] Javed, A., A. Arif, M. Zubair, M. Q. Mehmood, and K. Riaz, "A low-cost multiple complementary split-ring resonator-based microwave sensor for contactless dielectric characterization of liquids," *IEEE Sensors Journal*, Vol. 20, No. 19, 11 326–11 334, Oct. 2020.

[32] Kiani, S., P. Rezaei, and M. Navaei, "Dual-sensing and dual-frequency microwave srr sensor for liquid samples permittivity detection," *Measurement*, Vol. 160, 107805, 2020.

[33] Shafi, K. T. M., A. K. Jha, and M. J. Akhtar, "Dual band RF sensor for testing of magnetic properties of materials using meandered line SRR," *Sensors and Actuators A: Physical*, Vol. 272, 170–177, Apr. 2018.

[34] Buragohain, A., G. S. Das, Y. Beria, A. J. A. Al-Gburi, P. P. Kalita, and T. Doloi, "Highly sensitive differential hexagonal split ring resonator sensor for material characterization," *Sensors and Actuators A: Physical*, Vol. 363, 114704, Dec. 2023.

[35] Liu, W., J. Zhang, and K. Huang, "Dual-band microwave sensor based on planar rectangular cavity loaded with pairs of improved resonator for differential sensing applications," *IEEE Transactions on Instrumentation and Measurement*, Vol. 70, 1–8, 2021.

[36] Anggradinata, H. N. and M. Asvial, "Multifunctional dual-band microwave sensor for the detection of liquid permittivity and solid displacement," *Progress In Electromagnetics Research C*, Vol. 152, 131–141, 2025.

[37] Shi, H., X. Zhang, L. Huang, K. Wang, and Z. Wang, "Dual-band planar microwave solid complex dielectric constant sensor system based on E-interdigital structure," *Sensors*, Vol. 25, No. 18, 5789, Sep. 2025.

[38] Alam, S., Z. Zakaria, I. Surjati, N. A. Shairi, M. Alaydrus, and T. Firmansyah, "Dual-band independent permittivity sensor using single-port with a pair of U-shaped structures for solid material detection," *IEEE Sensors Journal*, Vol. 22, No. 16, 16 111–16 119, Aug. 2022.

[39] Alam, S., Z. Zakaria, I. Surjati, N. A. Shairi, M. Alaydrus, and T. Firmansyah, "Integrated microwave sensor and antenna sensor based on dual T-shaped resonator structures for contact and noncontact characterization of solid material," *IEEE Sensors Journal*, Vol. 23, No. 12, 13 010–13 018, Jun. 2023.

[40] Pozar, D. M., *Microwave Engineering*, John Wiley & Sons, 2012.

[41] Joler, M., A. N. J. Raj, and J. Bartolić, "A simplified measurement configuration for evaluation of relative permittivity using a microstrip ring resonator with a variational method-based algorithm," *Sensors*, Vol. 22, No. 3, 928, 2022.

[42] Hanif, A., M. T. Islam, M. L. Hakim, T. Alam, H. Alsaif, A. A. Maash, M. S. Soliman, and M. S. Islam, "Compact maze-shaped meta resonator for high-sensitive S-band low permittivity characterization," *Sensing and Bio-Sensing Research*, Vol. 45, 100655, Aug. 2024.